

SOLAR HYDROGEN PRODUCTION: TECHNO-ECONOMIC EVALUATION OF CONCENTRATED SOLAR POWER PLANT AND HIGH-TEMPERATURE ELECTROLYSIS INTEGRATION

João H. S. Martins ¹, Timo Roeder ^{1,2}, Andreas Rosenstiel ^{1,2} and Nathalie Monnerie ¹

¹ German Aerospace Center (DLR), Institute of Future Fuels, Cologne (Germany)

² RWTH Aachen University, Faculty of Mechanical Engineering, Chair for Solar Fuel Production, Aachen (Germany)

Abstract

High-temperature electrolysis systems produce hydrogen with high electrical efficiency, but require additional thermal energy for steam generation. Thus, this study explores the thermal and electrical integration of a concentrated solar power (CSP) plant with a high-temperature electrolysis system. Medium-temperature heat (above 150 °C) from the solar plant can be used for water evaporation during steam electrolysis, reducing the electrical energy demand compared to low-temperature alternatives. The techno-economic performance of this integration is evaluated through quasi-dynamic numerical simulations for a 50 MW plant in Morocco. The model includes a parametric analysis to optimize the levelized cost of hydrogen (LCOH) by varying the solar multiple and storage capacity. Additionally, the solar-to-fuel efficiency and capacity factor are evaluated, with comparisons to other CSP- and photovoltaic-powered electrochemical hydrogen production pathways. Under current cost assumptions, the optimal configuration (solar multiple of 2.29 and storage capacity of 10.7 hours) results in an LCOH of 7.88 EUR kg⁻¹. In a 2030 cost scenario, a similar configuration yields an LCOH of 4.83 EUR kg⁻¹, a capacity factor of 48 %, and a solar-to-fuel efficiency over 12 %. Finally, the sensitivity analysis identifies the most critical economic parameters influencing the LCOH, and highlights further research needs to bring this integration concept closer to competing technologies.

Keywords: Parabolic trough collectors, Solid oxide electrolysis cell, Thermal energy storage, Solar hydrogen production, Thermal and electrical integration

1. Introduction

Global hydrogen use reached 95 Mt in 2022, predominantly for refining and industrial processes. Virtually all of this was produced through processes such as steam methane reforming, which generates significant greenhouse gas (GHG) emissions. Nonetheless, hydrogen is also recognized as a promising sustainable energy carrier with the potential to bridge gaps in the temporal and spatial availability of renewable energy. Beyond the energy sector, hydrogen and its derivatives hold great promise for replacing fossil fuels and decarbonizing sectors such as aviation, shipping, and hard-to-abate industries like steel, cement, and fertilizer production (IEA, 2022). To realize this potential, hydrogen production must be driven by low-carbon energy sources, notably solar and wind, requiring further technological advancements to become cost-competitive with conventional processes.

Moreover, renewable hydrogen plays a pivotal role in the European Union's (EU) policy for energy transition, achieving net-zero emissions, and fostering sustainable development in the frame of the EU Green Deal. The EU's REPowerEU Strategy sets an ambitious target of producing 10 Mt of hydrogen domestically and importing an additional 10 Mt by 2030. By 2050, the aim is for renewable hydrogen to meet approximately 10 % of the EU's energy needs, enabling significant decarbonization of energy-intensive industrial processes and the transport sector (European Commission, 2020). Furthermore, Braun et al. (2023) estimate that nearly half of the EU's projected hydrogen demand of 25.9 Mt in 2050 could be met through imports from the Middle East and North Africa (MENA) region. Countries such as Morocco, Algeria, Tunisia, Libya, Egypt, and Saudi Arabia are identified as key partners, given their renewable energy potential, low production costs, geographic proximity to Europe, and established cross-regional infrastructure.

In terms of solar energy, the three main methods for producing hydrogen are electrochemical, photochemical, and thermochemical (Hausseiner, 2022). The electrochemical pathway – mainly using alkaline (AEC) or proton exchange membrane electrolysis cells (PEMEC), compatible with electricity from concentrated solar power (CSP), photovoltaics (PV), or hybrid CSP/PV systems – is the most mature, boasting the highest maturity, as highlighted by the IEA (2022). Rosenstiel et al. (2021) compared these three solar-driven systems for providing electricity to an AEC, finding that PV and hybrid systems achieve comparable levelized costs of hydrogen (LCOH), as low as 3.42 and 2.61 EUR kg⁻¹ in present and outlook scenarios for Morocco, respectively, while the CSP/PV system using solar power towers (SPT) demonstrates a significantly higher capacity factor. Moreover, CSP and hybrid systems offer a key advantage over PV systems by delivering lower lifetime GHG emissions (Edenhofer et al., 2011).

Within the electrochemical pathway, using solar heat and electricity for high-temperature electrolysis (HTE) with solid oxide electrolysis cells (SOECs) shows promise for improving efficiency and reducing hydrogen production costs (Seitz et al., 2017). SOECs can split water with lower total energy demands and operate at temperatures between 700–1000 °C by combining heat and electricity (Laurencin and Mougin, 2015). Figure 1 illustrates the thermodynamic energy demand of the water-splitting reaction for typical operating temperature ranges of low-temperature electrolysis (LTE) and HTE. Conducting the reaction at temperatures exceeding the evaporation point of water, by providing thermal energy to the process, decreases the total enthalpy change ΔH inside the electrolyzer by the heat of evaporation ΔH_{evap} , thereby reducing the associated electrical energy consumption and potentially lowering hydrogen costs. Additionally, higher temperatures reduce cell resistance, enabling electrical efficiencies above 90 %. Since CSP facilities can cost-effectively supply renewable electricity and medium- to high-temperature heat for extended periods, due to their compatibility with thermal energy storage (TES) systems, their energy streams can complement SOEC operating conditions. Despite these benefits, research on integrating CSP with the-SOEC systems is still limited in both literature and industrial applications.

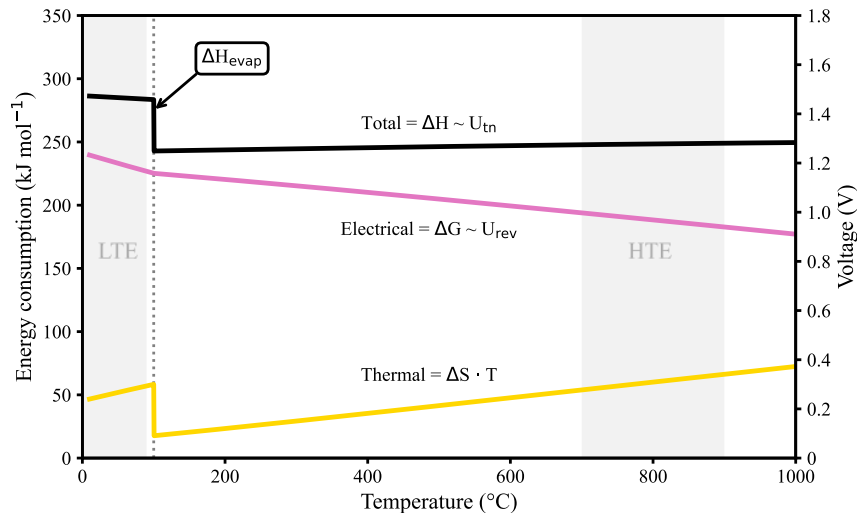


Fig. 1: Total energy demand of water splitting reaction at elevated temperature. U_{tn} = thermoneutral cell voltage; U_{rev} = reversible cell voltage. While LTEs usually operate under 100 °C, HTEs operate between 700–900 °C.

To address this, Immonen and Powell (2023) proposed three concepts for integrating solar energy with HTE-SOEC systems: (i) using PV and electrical heaters to meet both the electrical and thermal demands of the process; (ii) combining grid electricity with concentrated solar thermal (CST); and (iii) using CST and PV to meet the process's power and heat demands, respectively. Their study found similar LCOHs for all approaches, around 2.96 EUR kg⁻¹ in the USA, and concluded that achieving higher capacity factors, potentially through TES integration, is essential for meeting more ambitious cost targets, such as the Hydrogen Shot from the United States Department of Energy – of 1 USD kg⁻¹ (~ 0.93 EUR kg⁻¹) until the 2030s (DOE, 2023). Seitz et al. (2017) also explored a concept combining CST with SOECs modeled in Spain, achieving LCOHs of 3.67 EUR kg⁻¹ with TES and 5.33 EUR kg⁻¹ without TES. Another relevant study by Muhammad et al. (2024) carried simulations in EBSILON Professional to assess a CSP-SPT model to supply, under nominal conditions, 1–8 MW of electricity to an SOEC system, reporting LCOHs in the range of 5.64–8.23 EUR kg⁻¹ in Western

Australia. However, comprehensive studies evaluating the simultaneous provision of electricity and heat to an HTE-SOEC system exclusively by a CSP plant are still in the early stages, highlighting the need for further investigation, which this paper aims to address.

In this context, our study presents a techno-economic assessment (TEA) of electrically and thermally integrating a CSP plant using parabolic trough collectors (PTCs) with an HTE-SOEC system. We estimate the associated capacity factor, solar-to-fuel (STF) efficiency, and LCOH, comparing it to hydrogen production via electrochemical routes powered by CSP and/or PV listed above. To achieve this, we modeled and simulated the proposed hydrogen production plant over a typical meteorological year in Morocco, given the expected importance of MENA region in the European hydrogen supply chain.

2. Hydrogen plant description

The design, modeling and annual simulation of this solar-driven hydrogen production concept was performed by integrating two main process blocks – solar and electrochemical. The coupling was carried by combining built-in and user-defined macro components in EBSILON® Professional (STEAG, 2022) and Aspen Plus (AspenTech, 2021), enabling the evaluation of the hydrogen production plant under design and off-design conditions, as well as parametric analysis to be carried out to obtain the optimal LCOH, given various combinations of solar multiple and TES capacity. Figure 2 presents a simplified block diagram showing this integration and the main mass and energy flows.

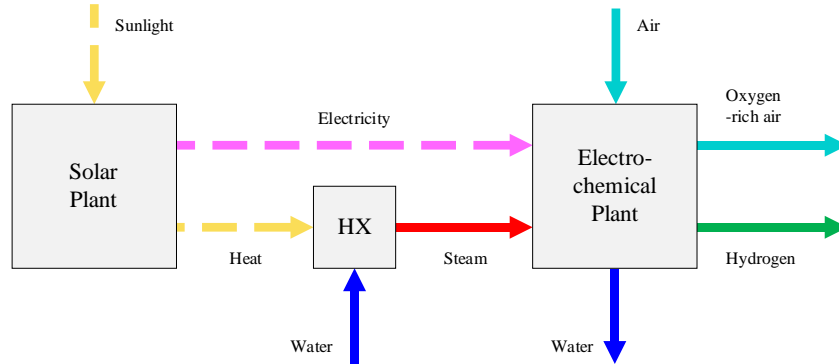


Fig. 2: Simplified scheme of the electrical and thermal integration of solar and electrochemical plants for hydrogen production. Full and dotted lines represent mass and energy streams, respectively. HX = heat exchanger.

The integrated model requires the characteristics of the solar and electrochemical sections as input, as well as the geographical and meteorological conditions of the selected site, here Ouarzazate in Morocco – where the world's largest CSP facility, the Noor Complex, is located (Thonig et al., 2023). Table 1 summarizes the important site parameters.

Tab. 1: Main geographical and meteorological parameters of the selected site (Meteotest, 2007). GHI = global horizontal irradiance; DNI = direct normal irradiance.

Parameter	Ouarzazate, MAR	Unit
Geographical coordinates	30.93; -6.90	° [latitude; longitude]
Elevation above sea level	1 140	m
Annual cumulative irradiation	2 123; 2 518	kWh m ⁻² [GHI; DNI]
Annual average ambient temperature	18.88	°C
Annual average wind speed	3.29	m s ⁻¹

The outputs of the numerical model are the profile of the heat and electricity dispatch from the CSP-PTC plant, as well as the water demand and hydrogen production of the HTE-SOEC system. For simplicity, the following technical assumptions were considered:

- Quasi-dynamic simulations with hourly timestep considered;
- Pressure drop and thermal losses in the piping are neglected;
- Thermal losses in the TES are neglected;
- An ideal linear HTE-SOEC partial load behavior is assumed; and
- Energy demand for hydrogen separation and further compression is neglected.

2.1. Solar plant

The solar plant layout is based on Andasol-1, the first commercial CSP-PTC facility to operate in Europe, and detailed by Feldhoff et al. (2012) and NREL (2013). It mainly consists of three hydraulic circuits: a synthetic oil circuit heated by the parabolic trough solar field; a molten salt circuit consisting of two indirectly integrated tanks for sensible heat storage, and a water/steam circuit for a conventional Rankine cycle. The main parameters of the solar plant are presented in Table 2.

Tab. 2: Nominal parameters of the solar plant for a SM=1 and storage capacity of one full-load hour.

Parameter	Value	Unit
Solar field		
SCA model	Eurotrough ET150	-
Number of SCAs	294	-
SCA dimensions	5.76; 150.00	m [<i>width; length</i>]
SCA aperture area	864.00; 817.43	m ² [<i>gross; net</i>]
Optical efficiency at design	74.73	%
Thermal efficiency at design	93.37	%
Solar field efficiency at design	69.77	%
HTF	Therminol VP-1	-
HTF temperature	290; 395	°C [<i>inlet; outlet</i>]
HTF pressure	5; 3.5	MPa [<i>inlet; outlet</i>]
Peak optical efficiency	75	%
Thermal energy storage		
HSM	Solar Salt	-
HSM temperature	385; 282	°C [<i>hot tank; cold tank</i>]
HSM mass capacity in each tank	3 600 000	kg
HSM mass flow rate at discharging	1 000	kg s ⁻¹
State of charge at beginning of simulation	50	%
Power block		
Steam temperature at turbine	373; 41	°C [<i>inlet; outlet</i>]
Water temperature at condenser	20; 36.5	°C [<i>inlet; outlet</i>]
Steam pressure at turbine	10; 0.008	MPa [<i>inlet; outlet</i>]
Steam pressures at extractions	4; 1.7; 0.6; 0.25; 0.12; 0.06	MPa [<i>extraction 1 to 6</i>]
Thermal energy demand	147	MW
Electric output	54.1; 50	MW [<i>gross; net</i>]
Thermal efficiency	38.1	%
Generator efficiency	96.00	%

The model for the solar field comprises a series of solar collector assemblies (SCA) of PTCs. They are used to increase the temperature of the Therminol VP-1 up to 395 °C, since this heat transfer fluid (HTF) suffers thermal degradation at higher temperatures. The sizing of the solar plant followed the design point method, described by Wang (2019). For a solar multiple $SM = 1$ – i.e., when solar field aperture area equals the area required to absorb the heat to run the power block in nominal conditions – a thermal capacity of 147 MW is required to achieve the electricity production of 54.1 MW gross and 50 MW net. This capacity was chosen to align with the scale of numerous existing installations, particularly in Spain (Thonig et al., 2023), ensuring practical implementation. This approach facilitates seamless integration with current CSP infrastructure, as only the SOEC system, including the heat exchanger, would need to be installed. CSP-PTC plants, with their modular design, offer simpler scalability than SPT plants and can potentially benefit from even larger capacities. However, while scaling up these plants could lead to cost reductions through economies of scale, this aspect is beyond the scope of the current study and will be addressed in the future.

The heat absorbed in the solar field can be stored in the TES using a heat storage medium (HSM) hydraulic circuit, composed of two tanks where Solar Salt – a mixture of 60 wt% of sodium nitrate (NaNO₃) and 40 wt% of potassium nitrate (KNO₃) – is kept at 385 °C and 282 °C in the hot and cold tanks, respectively. The resultant process flow diagram is shown ahead in Figure 4.

Finally, the power block is composed of a conventional Rankine cycle with steam input at 373 °C and 10 MPa, with net electrical capacity of 50 MW. The generator coupled to the steam turbine produces the electricity dispatched to the HTE system in addition to the electricity demanded by the balance of the plant (BOP) equipment, i.e., the pumps, compressors and electric heaters.

2.2. Electrochemical system

The electrolyzer design is based on a commercial model, the Sunfire-HyLink SOEC (Sunfire, 2021), modeled under thermoneutral operation, so lowest degradation rates are achievable (Lang et al., 2020) and heat can be efficiently recuperated, limiting the amount of external heat input for the superheating the HTE input streams (Petipas et al., 2014). The modeling of the electrolysis system was done in ASPEN Plus to integrate heat from the CSP plant efficiently, and was designed to reduce electrical requirements and enhance heat recovery from the electrolysis outlet streams. The HTE system is composed mainly of the SOEC, and a series of components such as heat exchangers, air compressors, electric heaters and gas coolers, responsible for providing air and steam at 820 °C and 0.6 MPa, as well as separating the hydrogen from the steam/hydrogen mixture at its outlet, while recuperating part of the heat from the outlet gases.

The results of the ASPEN Plus are used in the EBSILON Professional for the time series analysis. For the calculation of the electrical energy an electrical heater efficiency of 95 % (Kanthal, 2023) and a pumping and compressing efficiency of 98 % for the reagent gases of the electrolysis is assumed. Furthermore, the electrolysis efficiency is assumed to be 95.7 % for an isothermal operation at a steam conversion rate of 70 % (Tomberg et al., 2023). Then, the electrolysis system and thermal energy demands were calculated to match the net electric load for a conventional 50 MW CSP-PTC plant.

Once electricity and steam are produced, they are directed to the HTE system, which requires electricity, steam, air, and hydrogen inputs, as shown in Figure 2. The design point conditions for the HTE system are showed in Table 3. For off-design operation, when electricity and steam are provided in partial load, it was considered linear behavior, assuming that even in part load operation, a share of the electrolyzer stacks is operated in nominal conditions. For the inactive stacks, a hot standby mode is considered, in which an electrical demand equivalent to 8.2 % of their nominal requirement is used to avoid temperature drop during inactivity. Since during these periods of inactivity, the CSP plant is unable to provide the input for the hot standby mode, it is provided by the connection with the electrical grid.

Tab. 3: Nominal parameters of the electrochemical plant.

Parameter	Value	Unit
Total electrical input	50	MW
SOEC electrical demand	47.27	MW
Electric heater demand	2.34	MW
BOP electrical demand	0.40	MW
SOEC temperature	850; 820	°C [<i>inlet; outlet</i>]
Steam/water mass flow rate	2.486; 0.746	kg s ⁻¹ [<i>inlet; outlet</i>]
Air mass flow rate	8.303; 2.099	kg s ⁻¹ [<i>inlet; outlet</i>]
Air mass flow rate	0.058; 0.424	kg s ⁻¹ [<i>inlet; outlet</i>]
Net hydrogen production rate	0.366	kg s ⁻¹
Steam conversion rate	70	%
SOEC nominal efficiency	95.7	%
SOEC electricity demand on hot standby mode	8.2	% nominal demand
SOEC electricity demand at end of life	105	% nominal demand
H ₂ content at SOEC inlet steam-H ₂ stream	10	mol%
O ₂ content at SOEC outlet O ₂ -rich air stream	40	mol%

2.3. Operation strategy

To represent the operation of the hydrogen production plant in multiple conditions throughout a typical year, the plant control model developed in EBSILON at the EbsScript interface accounted for five operation modes. The decision tree of the operation strategy is summarized in Figure 3.

Those steps are carried for each timestep of the simulation and decide the operation of the solar field, TES, power block, and the electrical and thermal dispatch from the CSP plant to the HTE-SOEC system. Moreover, the dispatch strategy was modeled to run the hydrogen plant in full-load as long as possible.

- Mode 1: the solar field charges the TES and supplies heat and electricity to the HTE. Hydrogen is produced in full- or part-load and the TES's state of charge (SoC) increases;
- Mode 2: the available heat is not enough to simultaneously charge the TES and power the HTE, thus the HTE is prioritized. Hydrogen is produced in full- or part-load and the TES's SoC is unaltered;
- Mode 3: due to low solar irradiance, the solar field is supported by the TES in supplying heat and electricity to the HTE. Hydrogen is produced in full- or part-load and the TES's SoC decreases;
- Mode 4: the solar irradiance in the solar field is insufficient to drive the process and the TES is not completely discharged. Thus, heat and electricity are supplied to the electrolysis exclusively by the TES. Hydrogen is produced in full- or part-load and the TES's SoC decreases;
- Mode 5: the solar irradiance in the solar field is insufficient to drive the process and the TES is completely discharged. Hydrogen is not produced and the TES's SoC stays at its minimum.

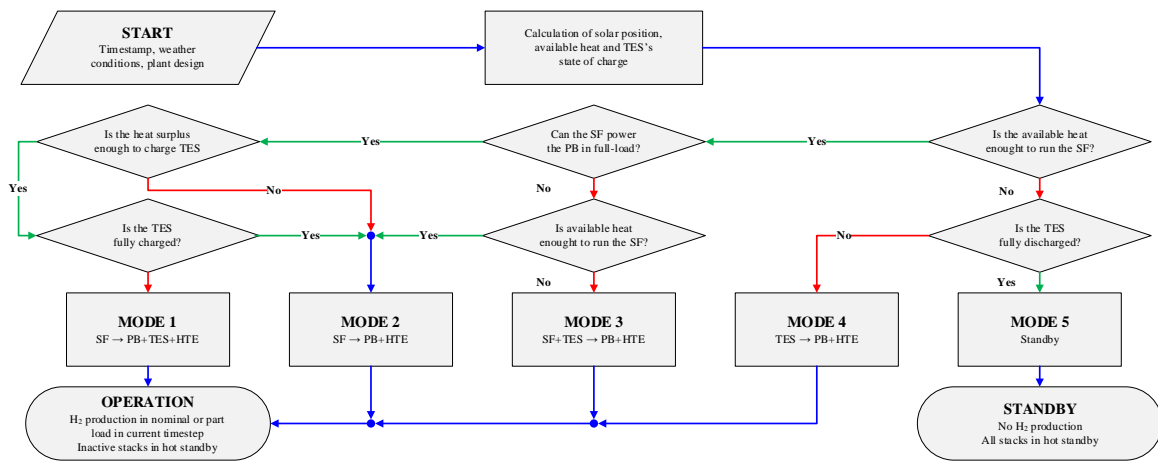


Fig. 3: Visual scheme of the operation strategy decision. SF = solar field; PB = power block.

2.4. Parametric analysis

To complement the modeling of the plant, a parametric analysis evaluates how changing input variables affects the output of a model. In this study, the focus was on how varying the solar field size – given by the solar multiple – and TES capacity influences the process KPIs. The analysis involved simulating various combinations of SMs (ranging from 1 to 4) and TES capacities (ranging from no storage to 18 hours of equivalent full load operation). After that, those discrete results undergo through an interpolation algorithm to obtain continuous values for all KPIs, which are used to identify the plant configurations with the highest capacity factor, STF efficiency and, above all, the lowest LCOH – which indicates the most cost-effective configuration for the hydrogen production plant.

3. Techno-economic modeling

The methodology used for the techno-economic analysis largely follows the approach outlined by Albrecht et al. (2017). Key performance indicators (KPI) are established to assess the efficiency, energy conversion, and economic viability of the hydrogen production process, alongside the economic boundary conditions that define our analysis.

3.1. Key performance indicators

The primary KPIs evaluated include the capacity factor (CF), solar-to-fuel efficiency (η_{STF}) and the LCOH. The capacity factor reflects how effectively the process operates relative to its maximum potential output. It is calculated as the ratio between the actual hydrogen output $\sum_{t=1}^n H_{2,t}$ and the theoretical maximum output over a given period if the process were running at full capacity $H_{2,design}$. Given the assumption of process

degradation, this calculation extends across the entire plant lifetime n of 25 years. The contribution of each year is denoted by the subscript t .

$$CF = \frac{\text{Actual H}_2 \text{ output [kg]}}{\text{Theoretical maximum H}_2 \text{ output [kg]}} = \frac{\sum_{t=1}^n H_{2,t}}{8760 \cdot n \cdot H_{2,design}} [-] \quad (\text{eq. 1})$$

The STF efficiency η_{STF} is defined as the ratio of the energy content of the produced fuel, based on the lower heating value of hydrogen LHV_{H_2} , to the incident solar energy in the solar field Q_{solar} plus the auxiliary electricity from the grid E_{aux} . Similar to the capacity factor, it was calculated throughout the plant lifetime.

$$\eta_{STF} = \frac{\text{Total energy stored at the produced H}_2 \text{ [J]}}{\text{Total energy provided to the process [J]}} = \frac{\sum_{t=1}^n H_{2,t} \cdot LHV_{H_2}}{\sum_{t=1}^n (Q_{solar,t} + 2.5 \cdot E_{aux,t})} [-] \quad (\text{eq. 2})$$

Finally, the LCOH is the cost the per-unit of producing hydrogen, considering all capital, operational, and maintenance expenses over the facility's lifetime. Here it was calculated using the cash flow method. The detailed procedure for this calculation and definitions of engineering, procurement, and construction (EPC) costs, capital expenditure (CAPEX), operating expenditure (OPEX), and interest rate i are further described by Dersch et al. (2020), containing detailed cost parameters for 2018 and 2030 for different locations.

$$LCOH = \frac{\text{Total life cycle costs [EUR]}}{\text{Total life cycle H}_2 \text{ production [kg]}} = \frac{\sum_{t=0}^n (CAPEX_t + OPEX_t)(1+i)^{-t}}{\sum_{t=1}^n (H_{2,t})(1+i)^{-t}} [\text{EUR kg}^{-1}] \quad (\text{eq. 3})$$

The process STF efficiency, capacity factor, heat, electricity and hydrogen production results from the time series calculations from EBSILON are used for performing the TEA, in which the CAPEX and fixed annual OPEX are used for the LCOH calculation. This LCOH is then used as the main performance indicator for the comparison with other hydrogen production technologies.

3.2. Cost assumptions

The main cost parameters used for the TEA calculations are summarized in Table 4. It is noteworthy that the costs and energy demand for hydrogen compression are neglected, while an annual interest rate of 7.5 % and a plant lifetime of 25 years are assumed.

Tab. 4: Cost parameters considered for the TEA in 2023 and 2030 scenarios.

Parameter	2023	2030	Unit
Direct EPC costs			
Solar field	247	150	EUR m ⁻² aperture
Thermal energy storage	49	24	EUR kWh ⁻¹
Power block	935	638	EUR kW ⁻¹
High-temperature electrolyzer	3 270	1 566	EUR kW ⁻¹
Indirect EPC costs			
Engineering, management, EPC services	5	2	% total EPC
Profit margin and contingencies	10	6	% direct EPC
Owner's costs			
Infrastructure (grid connection, roads, etc.)	5 550 000	5 550 000	EUR
Project development	4	2	% total EPC
Additional owner's cost	3	2	% total EPC
Specific land cost	0.93	0.93	EUR m ⁻² land
Running costs			
Annual CSP O&M cost	1.5	1.5	% CSP direct EPC
Annual HTE O&M cost	32.5	12.5	EUR kW ⁻¹
SOEC stack replacement cost	$f(CF)$	$f(CF)$	EUR kW ⁻¹
SOEC stack durability	$f(CF)$	$f(CF)$	a
Annual insurance cost	0.7	0.7	% direct EPC
Electricity cost	93	93	EUR MWh ⁻¹
Water costs	2	2	EUR m ⁻³

The cost assumptions for the CSP plant were obtained from the study by Dersch et al. (2020), which presents the costs for the components of a CSP-PTC plant and its site-specific costs when implemented in several countries. The costs were adjusted to Morocco using a price index of 42, as well as local and global cost shares. Moreover, all costs are converted to EUR₂₀₂₃ using the Chemical Engineering Plant Cost Index (CEPCI). Finally, the average exchange rate of the reference year for converting costs between USD and EUR.

The total SOEC system investment cost is calculated with a methodology from a previous study (Roeder et al., 2024). Its cost calculation method considers cost development predictions from Böhm et al. (2020) and stack lifetime development expectations from various studies and reports. Thus, the year of the stack replacement and the individual costs as a function of process capacity factor (or full load hours) and project lifetime is calculated. Additionally, annual operation and maintenance (O&M) costs for the electrolysis system are considered as in Smolinka et al. (2018). The O&M costs are considered to be constant throughout the project lifetime because, they are considered for the whole HTE system.

4. Simulation results and discussion

The key findings from the simulation of the integrated hydrogen production process are presented below. The plant integration is first examined, with a focus on how the solar and electrochemical systems were combined. Next, the capacity factor and solar-to-fuel efficiency are discussed, highlighting how operational conditions affect system performance. Finally, the levelized cost of hydrogen (LCOH) is analyzed, followed by a sensitivity analysis to identify the factors most influencing this critical indicator.

4.1. Plant integration

The outcome of the design of the integrated process is presented in Figure 4, which shows the schematic process diagram. In the presented concept, the solar and electrochemical systems are integrated through a heat exchanger that extracts heat from the synthetic oil at the outlet of the power block at a temperature around 290 °C, in line with the simplified diagram shown in Figure 2. In addition, the main parameters from the simulation of the heat exchanger used for steam generator are contained in Table 5.

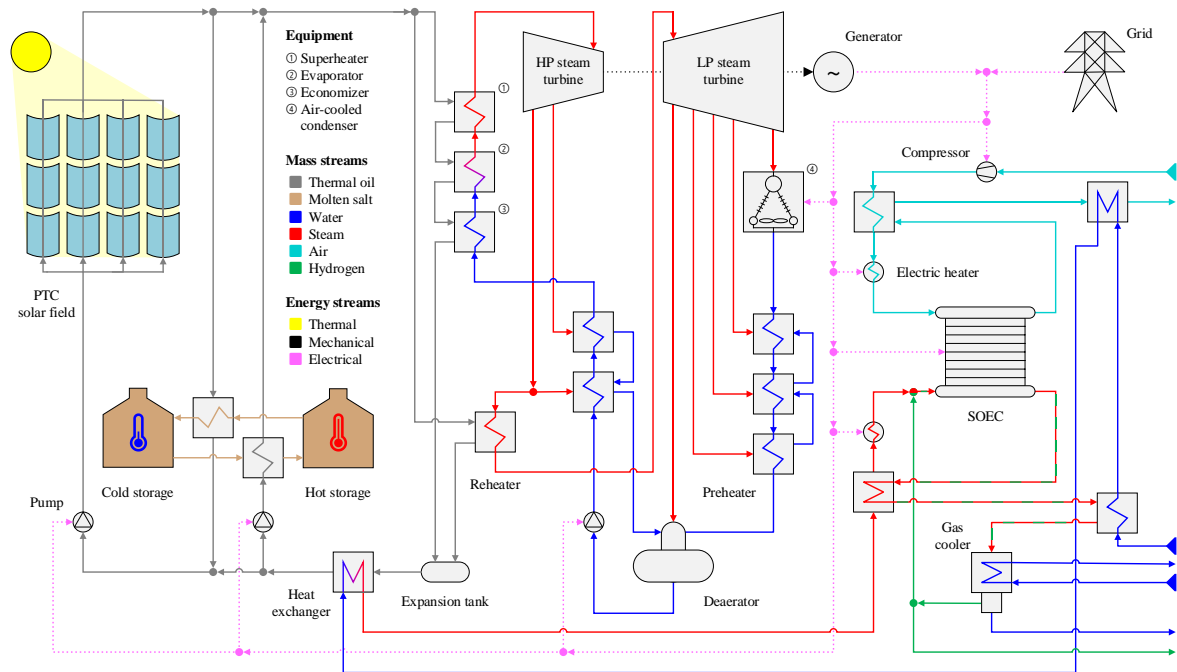


Fig. 4: Scheme of the thermal and electrical integration between PTC-CSP plant and HTE-SOEC system for solar hydrogen production, highlighting main equipment, mass and energy streams. Grid connection is used only for SOEC hot standby. LP = low pressure; HP = high pressure.

After the steam generation, electricity is used to reach the water-splitting temperature around 850 °C under SOEC thermoneutral operation, which is favorable for long stack lifetimes (Lang et al., 2020). This choice simplifies the combined operation of the power block with the HTE, which requires proportional amounts of

steam and electricity for hydrogen production. In addition, this integration position does not interfere with the water/steam cycle, which can significantly change the operating point and performance of the steam turbine. Furthermore, this solution has the potential to be retrofitted into existing CSP-PTC plant, requiring only minor changes in the system design.

Tab. 5: Parameters of the integrated steam generator.

Parameter	Value	Unit
Thermal oil temperature	292; 286	°C [<i>inlet; outlet</i>]
Water/steam temperature	95; 200	°C [<i>inlet; outlet</i>]
Thermal oil pressure	1.5; 1.45	MPa [<i>inlet; outlet</i>]
Water/steam pressure	0.65; 0.6	MPa [<i>inlet; outlet</i>]
Water/steam mass flow rate at design	4.67	kg s ⁻¹
Thermal energy demand	9.463	MW

4.2. Capacity factor

The capacity factors resulting from the process simulation are shown in Figure 5 (a) and (b), reflecting the CSP-HTE performance for 2023 and 2030, respectively. With expected improvements in SOEC durability over time, the average SOEC lifetime is expected to increase for the future scenario, which leads to lower electrical demand and/or reduced hydrogen output, causing a slight increase in the process capacity factor from 61.75 % in 2023 to 62.20 % in 2030. The maximum capacity factor is achieved with a combination of 18 hours of storage capacity and a solar multiple of approximately 3.4.

These results align with the known relationship between storage capacity and solar multiple, indicating that both must be increased proportionally to achieve higher capacity factors. Otherwise, the solar field cannot provide sufficient heat for disproportionate large storage systems, or the excess heat from an oversized solar field cannot be efficiently stored.

4.3. Solar-to-fuel efficiency

Similar to the results for the capacity factor, the values for the STF efficiency are summarized in Figure 5 (c) for 2023 and (d) for 2030. It is observed that the peak efficiency values do not align with the highest capacity factors, and are generally achieved for combinations of intermediate solar multiples and storage capacities. While higher solar multiples and larger storage can enhance the plant's ability to produce hydrogen consistently, they can also lead to inefficiencies, such as excess heat that cannot be effectively converted or stored. This discrepancy occurs because optimizing for continuous operation and maximizing output does not always match the conditions that yield the highest conversion efficiency. For example, the process may be less efficient when powered by heat from the TES due to lower temperatures when compared to the heat provided directly by the solar field, and during part-load conditions, where power block efficiency decreases at lower steam mass flow rates, temperatures, or pressures.

In our simulations it was obtained similar maximum efficiencies for 2023 and 2030, about 12 % for a combination of solar multiple of 2.41 and 5.51 hours of storage. The value is slightly increased in 2030 mainly due to reduced degradation expected for the SOEC stacks, resulting in a lower average specific electrical consumption by the stacks over their lifetime. This improvement for the future scenario could be further improved if enhancements of the CSP performance (e.g., higher HTF temperature, more efficient power blocks and/or SCAs) are considered.

4.4. Levelized cost of hydrogen

Finally, the results of the LCOH for various combinations of solar multiple and storage capacity are presented in Figure 5 (a) for 2023 and (b) for 2030. We considered it as the most important indicator, since it allows comparison with other hydrogen production processes and cost targets. For the 2023 scenario, which includes higher specific costs for purchasing and maintaining the solar and electrochemical components of the plant and decreased durability of the stacks in the HTE-SOEC system, the minimum LCOH is significantly higher compared to the 2030 scenario. The 2030 scenario benefits from more favorable technical and economic conditions. Specifically, for 2023, the lowest achieved LCOH is 7.88 EUR kg⁻¹ with a solar multiple of 2.29 and 10.65 hours of storage. In contrast, for 2030, the LCOH decreases to 4.83 EUR kg⁻¹ with a solar multiple of 2.35 and the same storage capacity.

The analysis also suggests that storage capacities exceeding 18 hours could potentially lead to even lower LCOHs. However, due to their extensive size, storage capacities beyond that were not evaluated in this study, and could be the subject of future studies. Additionally, improvements in CSP plant performance and economy of scale factor for component costs could further reduce the LCOH. These factors were not included in our study but could further lower the optimal LCOH, especially if larger storage and more extensive solar fields were used.

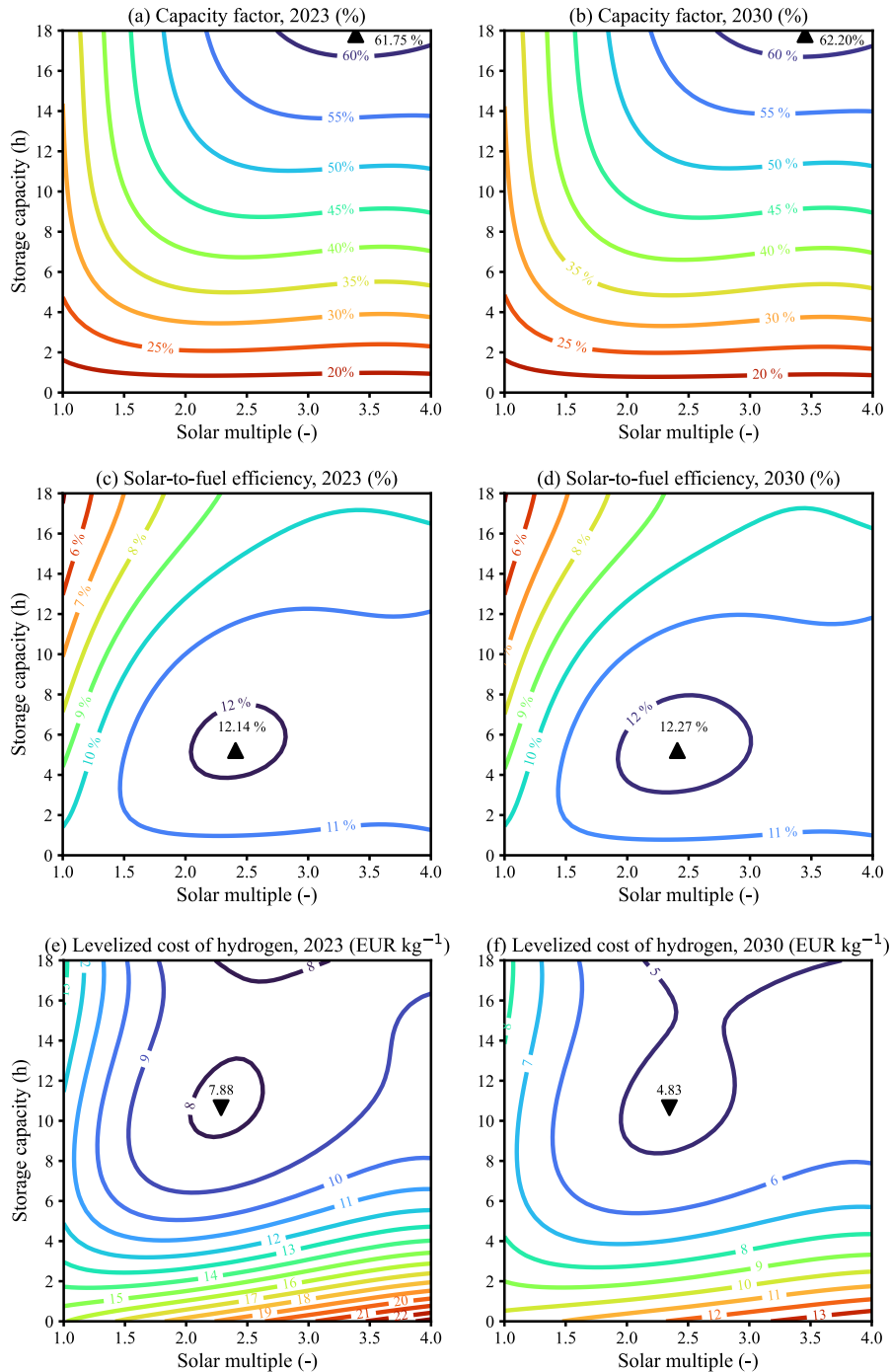


Fig. 5: Isolines for the key performance indicators of the process according to different combinations of solar multiple and storage capacity considering current (2023) and future (2030) assumptions. Capacity factor for 2023 (a) and 2030 (b); Solar-to-fuel efficiency using hydrogen’s LHV for 2023 (c) and 2030 (d); and levelized cost of hydrogen for 2023 (e) and 2030 (f).

Compared to the literature reviewed in the introduction section, which reports LCOHs ranging from 2.61 to 8.23 EUR kg⁻¹, our model yields comparable results for both current and future scenarios, but costs remain higher than the lowest LCOH identified. Nevertheless, this direct comparison is not simple, as relevant disparities are present in LCOH calculation methods, site-specific meteorological conditions, and differing

economic assumptions, including the use of different base years for economic analyses. Since our study adjusts cost assumptions for inflation, it is expected to produce less competitive but realistic results. Further improvements in the process, TEA methodology, and comparisons under consistent boundary conditions could provide clearer insights into the advantages and disadvantages of each process.

4.5. Sensitivity analysis

After the parametric analysis, a sensitivity analysis was conducted to further explore how varying key input variables affect the LCOH. Figure 6 presents a detailed sensitivity analysis, showing the impact of nine variables on LCOH for both 2023 and 2030 scenarios. These variables include interest rates, cost of components, O&M, and utilities.

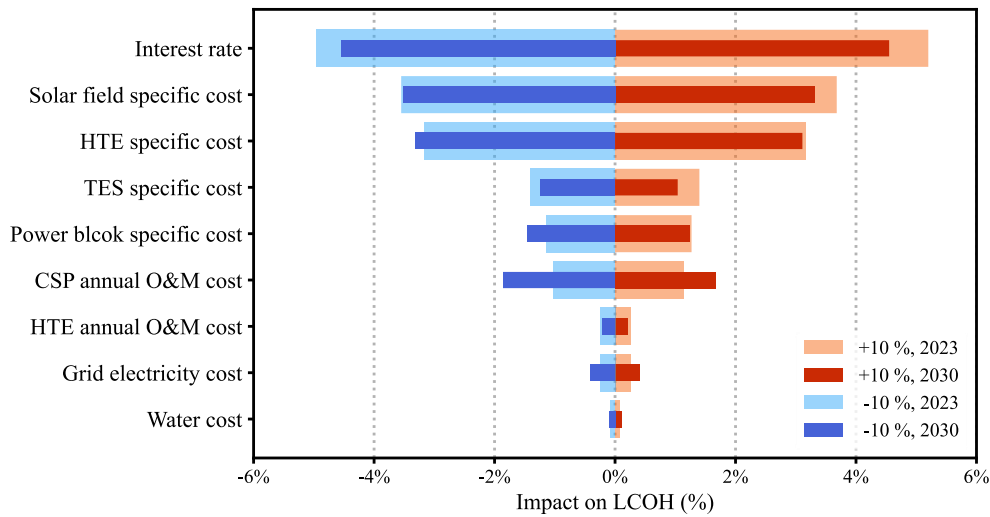


Fig. 6: Sensitivity of the LCOH on the variation of selected input variables in $\pm 10\%$ considering the 2023 and 2030 scenarios.

It was found that while sensitivity patterns remain consistent between the 2023 and 2030 scenarios, the impact range for some variables varies more significantly. The most significant influence on LCOH is the interest rate; reducing it by 10% results in a 4.6% decrease in LCOH for 2023 and a 5% decrease for 2030. Fluctuations in the interest rate beyond this are common, underscoring its importance in evaluating the cost-effectiveness of this capital-intensive technology. For example, if the interest rate changes from 7.5% (the value considered in our study) to 5%, the LCOH decreases to 6.61 EUR kg⁻¹ for 2023 and 4.13 EUR kg⁻¹ for 2030. Following interest rates, the next most relevant parameters identified were the specific costs of the solar field and the HTE system, reinforcing the significant influence of the uncertainties in cost projections of both systems to the quality of such TEA studies.

After interest rates, the specific costs of the solar field and the HTE system emerge as the most critical parameters, highlighting how uncertainties in the cost projections of both systems can significantly impact the quality of TEA studies and make direct comparisons with literature challenging.

Conversely, variables such as the water, grid electricity and the O&M costs for the HTE and CSP systems exhibit less significant impact on LCOH in both scenarios. The bars representing these variables are comparatively short, indicating that changes in these factors have a relatively small effect on the overall LCOH.

5. Conclusions and outlook

This study provides a comprehensive techno-economic analysis of integrating a concentrated solar power (CSP) plant using parabolic trough collectors and high-temperature electrolysis using solid oxide electrolysis cells for hydrogen production, focusing on Ouarzazate, Morocco. Through numerical simulations in EBSILON Professional and ASPEN Plus, we assessed the performance, efficiency, and costs of this system, uncovering several key findings and possibilities for further research.

Effective thermal and electrical integration between the CSP plant and the electrolysis system was evident from the schematic process flow diagram and performance parameters, demonstrating promising efficiency

and cost-effectiveness. The system achieved a peak capacity factor of approximately 61.75 % in 2023, projected to slightly rise to 62.20 % by 2030, reflecting anticipated improvements in electrolysis cell durability. Although the peak solar-to-fuel efficiency peak, around 12 %, did not correspond with the highest capacity factors, it highlighted the need for a trade-off between continuous operation and efficiency. Simultaneously, the levelized cost of hydrogen (LCOH) decreased significantly from 7.88 EUR kg⁻¹ in 2023 to 4.83 EUR kg⁻¹ by 2030, demonstrating the economic benefits of technological advancements and enhanced system performance and economics. Finally, the sensitivity analysis revealed that factors like interest rates and solar field and electrolysis cells specific costs play a big role in the LCOH due to the process capital intensity.

Future research ought to explore several areas aiming to further optimize the synergies of solar and high-temperature electrolysis systems. Integrating photovoltaic systems to the CSP plant could enhance energy output and efficiency by providing additional low-cost electricity and increasing thermal energy storage temperatures. Additionally, using solar power towers in CSP plants could offer both electricity and higher-temperature heat, potentially improving operational efficiency and reducing even more the electrolysis electrical consumption. Moreover, comparing this production pathway with alternative hydrogen production methods, evaluating the impact of scale, location, and technological advancements of CSP on future scenarios will be crucial for refining cost predictions and enhancing economic feasibility assessment, potentially make it even more attractive and able to outperform competitor technologies, and therefore will follow in next studies. Finally, a life-cycle assessment of such system could potentially shed light not only its economic benefits but also its environmental advantages, leveraging one of the key strengths of CSP and CST technologies. Addressing these aspects will advance efficient and cost-effective hydrogen production, leveraging solar energy sustainably.

6. Acknowledgments

Financial support from DLR's basic funding for the project NeoFuels is gratefully acknowledged.

7. References

- Albrecht, F.G., König, D.H., Baucks, N., Dietrich, R.-U., 2017. A standardized methodology for the techno-economic evaluation of alternative fuels – A case study. *Fuel* 194, 511–526. doi: 10.1016/j.fuel.2016.12.003.
- AspenTech, 2021. Aspen Plus Version 12.1. Aspen Technology Inc, Bedford, USA.
- Böhm, H., Zauner, A., Rosenfeld, D.C., Tichler, R., 2020. Projecting cost development for future large-scale power-to-gas implementations by scaling effects. *Applied Energy* 264, 114780. doi: 10.1016/j.apenergy.2020.114780.
- Braun, J., Frischmuth, F., Gerhardt, N., Pfenning, M., Schmitz, R., Wietschel, M., Carlier, B., Réveillère, A., Warluzel, G., Wesoly, D., 2023. Clean Hydrogen Deployment in the Europe-MENA Region from 2030 to 2050.
- Dersch, J., Dieckmann, S., Hennecke, K., Pitz-Paal, R., Taylor, M., Ralon, P., 2020. LCOE reduction potential of parabolic trough and solar tower technology in G20 countries until 2030, in: SOLARPACES 2019: International Conference on Concentrating Solar Power and Chemical Energy Systems, Daegu, South Korea. 1–4 October 2019. AIP Publishing, 120002. doi: 10.1063/5.0028883.
- DOE, 2023. U.S. National Clean Hydrogen Strategy and Roadmap. U.S. Department of Energy, Washington, USA. <https://www.hydrogen.energy.gov/library/roadmaps-vision/clean-hydrogen-strategy-roadmap> (accessed on Nov 2024).
- Edenhofer, O., Pichs-Madruga, R., Sokona, Y., Seyboth, K., Matschoss, P., Kadner, S., Zwickel, T., Eickemeier, P., Hansen, G., Schlömer, S., Stechow, C. von (Eds.), 2011. IPCC Special Report on Renewable Energy Sources and Climate Change Mitigation. Cambridge University Press, Cambridge, United Kingdom and New York, NY, USA.
- European Commission, 2020. A hydrogen strategy for a climate-neutral Europe, Brussels, Belgium. <https://eur-lex.europa.eu/legal-content/EN/TXT/?uri=CELEX:52020DC0301> (accessed on Nov 2024).
- Feldhoff, J.F., Schmitz, K., Eck, M., Schnatbaum-Laumann, L., Laing, D., Ortiz-Vives, F., Schulte-Fischedick, J., 2012. Comparative system analysis of direct steam generation and synthetic oil parabolic

trough power plants with integrated thermal storage. *Solar Energy* 86, 520–530.
doi: 10.1016/j.solener.2011.10.026.

Haussener, S., 2022. Solar fuel processing: Comparative mini-review on research, technology development, and scaling. *Solar Energy* 246, 294–300. doi: 10.1016/j.solener.2022.09.019.

IEA, 2022. *Global Hydrogen Review 2022*. International Energy Agency, Paris, France.

Immonen, J., Powell, K.M., 2023. Hydrogen from solar? A rigorous analysis of solar energy integration concepts for a high temperature steam electrolysis plant. *Energy Conversion and Management* 298, 117759. doi: 10.1016/j.enconman.2023.117759.

Kanthal, 2023. *Flow Heaters - Information*. Kanthal AB. <https://www.kanthal.com/en/products/air-heaters/flow-heaters/> (accessed on Jan 2024).

Lang, M., Raab, S., Lemcke, M.S., Bohn, C., Pysik, M., 2020. Long-Term Behavior of a Solid Oxide Electrolyzer (SOEC) Stack. *Fuel Cells* 20, 690–700. doi: 10.1002/face.201900245.

Laurencin, J., Mougou, J., 2015. High-Temperature Steam Electrolysis, in: Godula-Jopek, A. (Ed.), *Hydrogen Production*. Wiley, pp. 191–272.

Meteotest, 2007. *Meteonorm Version 6.1*. Meteotest AG, Bern, Switzerland.

Muhammad, H.A., Naseem, M., Kim, J., Kim, S., Choi, Y., Lee, Y.D., 2024. Solar hydrogen production: Technoeconomic analysis of a concentrated solar-powered high-temperature electrolysis system. *Energy* 298, 131284. doi: 10.1016/j.energy.2024.131284.

NREL, 2013. *System Advisor Model (SAM) Case Study: Concentrating Solar Power (CSP) Physical Trough Andasol-1*. Boulder, USA.

Petipas, F., Brisse, A., Bouallou, C., 2014. Benefits of external heat sources for high temperature electrolyser systems. *International Journal of Hydrogen Energy* 39, 5505–5513. doi: 10.1016/j.ijhydene.2014.01.179.

Roeder, T., Rosenstiel, A., Monnerie, N., Sattler, C., 2024. Impact of expected cost reduction and lifetime extension of electrolysis stacks on hydrogen production costs. *International Journal of Hydrogen Energy*. doi: 10.1016/j.ijhydene.2024.08.015.

Rosenstiel, A., Monnerie, N., Dersch, J., Roeb, M., Pitz-Paal, R., Sattler, C., 2021. Electrochemical Hydrogen Production Powered by PV/CSP Hybrid Power Plants: A Modelling Approach for Cost Optimal System Design. *Energies* 14, 3437. doi: 10.3390/en14123437.

Seitz, M., Storch, H. von, Nechache, A., Bauer, D., 2017. Technoeconomic design of a solid oxide electrolysis system with solar thermal steam supply and thermal energy storage for the generation of renewable hydrogen. *International Journal of Hydrogen Energy* 42, 26192–26202. doi: 10.1016/j.ijhydene.2017.08.192.

Smolinka, T., Wiebe, N., Sterchele, P., Palzer, A., Lehner, F., Jansen, M., Kiemel, S., Mieke, R., Wahren, S., Zimmermann, F., 2018. *IndWEde: Industrialisierung der Wasserelektrolyse-Industrie in Deutschland*. Freiburg, Germany.

STEAG, 2022. *EBSILON®Professional Version 16.00*. STEAG Energy Services GmbH, Zwingenberg, Germany.

Sunfire, 2021. *Sunfire-HyLink SOEC Factsheet*. Sunfire GmbH. <https://www.sunfire.de/en/hydrogen> (accessed on Jan 2024).

Thonig, R., Gilmanova, A., Lilliestam, J., 2023. *CSP.guru 2023-07-01*. Zenodo. doi: 10.5281/zenodo.8191855.

Tomberg, M., Heddrich, M.P., Ansar, S.A., Friedrich, K.A., 2023. Operation strategies for a flexible megawatt scale electrolysis system for synthesis gas and hydrogen production with direct air capture of carbon dioxide. *Sustainable Energy Fuels* 7, 471–484. doi: 10.1039/D2SE01473D.

Wang, Z., 2019. General Design of a Solar Thermal Power Plant, in: *Design of Solar Thermal Power Plants*. Elsevier, pp. 117–224.